Subduction and atmospheric escape of Earth's seawater constrained by hydrogen isotopes

Hiroyuki Kurokawa *, Julien Foriel, Matthieu Laneuville, Christine Houser, Tomohiro Usui

Earth-Life Science Institute, Tokyo Institute of Technology, 2-12-1 Ookayama, Meguro, Tokyo 152-8550, Japan

A B S T R A C T

The hydrogen isotopic (D/H) ratio reflects the global cycling and evolution of water on Earth as it fractionates through planetary processes. We model the water cycle taking seafloor hydrothermal alteration, chemical alteration of continental crust, slab subduction, hydrogen escape from the early Earth, and degassing at mid-ocean ridges, hot spots, and arcs into account. The differences in D/H ratios between present-day oceans, oceanic and continental crust, and mantle are thought to reflect isotopic fractionation through seafloor alteration, chemical alteration, and slab dehydration. However, if the speed of plate tectonics has been nearly constant throughout Earth's history, the degassing and regassing rates are too small to reach the present-day D/H ratios. We show that (a) hydrogen escape from reduced early atmosphere, (b) secular net regassing, or (c) faster plate tectonics on early Earth is needed to reproduce the present-day D/H ratios of the water reservoirs. The low D/H ratio of Archean seawater at 3.8 Ga has previously been interpreted as a signature of (a) hydrogen escape, but we find it can also be explained either by (b) secular net degassing or by (c) faster plate tectonics on early Earth. The rates of hydrogen escape from early Earth and secular regassing on present-day Earth are constrained to be lower than 2.1×10^{11} kg/yr and 3.9×10^{11} kg/yr. Consequently, the volume of water in the present-day mantle could result entirely from the regassing through Earth's history. In that case, the volume of initial oceans could be 2 to 3 times larger than that of current Earth. We suggest that, in addition to the D/H ratio of Archean seawater, identifying the D/H ratios of both seawater and mantle throughout Earth's history would allow to distinguish these evolutionary scenarios.

© 2018 Elsevier B.V. All rights reserved.

1. Introduction

Water plays a critical role in controlling the physical and chemical evolution on Earth through atmosphere–ocean–continent interactions which control the atmospheric composition, the climate through the carbon cycle, the subduction of water, and possibly even the emergence and evolution of life (e.g., Gaillard et al., 2011; Walker, 1977; Höning et al., 2014; Höning and Spohn, 2016; Dohm and Maruyama, 2015). Furthermore, the abundance of water in Earth's interior influences the mantle melting, rheology, and style of convection (e.g., Hirschmann, 2006; Karato and Jung, 2003; Mei and Kohlstedt, 2000).

The abundance of water on the surface and in the interior is controlled by the deep water cycle between the oceans and mantle, and loss caused by hydrogen escape throughout Earth's history. Slab subduction transports water as bound and pore water in metamorphic rocks and sediments that originate from hydrother-

mal alteration of the seafloor and chemical alteration of continental crust (e.g., Jarrard, 2003; Bodnar et al., 2013; Höning et al., 2014; Höning and Spohn, 2016). While the majority of the subducted water returns to the oceans directly by updip transport and indirectly by arc volcanism, some trace amounts of water may remain in the mantle. Water can return from the mantle to the exosphere (here defined as the atmosphere and hydrosphere) by degassing at mid-ocean ridges and ocean islands. Although the photolysis of water has a negligible effect on the loss of hydrogen from the atmosphere today, the hydrogen escape through the photolysis of methane in the reduced early atmosphere before the great oxidation event (GOE) at 2.5 Ga could have a more significant impact (Catling et al., 2001).

Despite its importance to control the water budget, the balance between the degassing and regassing as well as the early hydrogen escape flux is poorly understood. We note that the term "regassing" means the water transport to the mantle as bound and pore water in metamorphic rocks and sediments. Net regassing from the oceans to the mantle has been suggested from the geochemical estimates (Ito et al., 1983). The continental freeboard is

proposed to be nearly constant from the end of the Archean (e.g., Schubert and Reymer, 1985) and is interpreted as the degassing and regassing rates almost achieving balance (e.g., Lécuyer et al., 1998; Parai and Mukhopadhyay, 2012). However, Korenaga et al. (2017) recently argued that the relative buoyancy of continental lithosphere with respect to oceanic lithosphere was higher in the past, which requires a larger volume of oceanic water at the time to keep continental freeboard constant. Hydrogen escape on early Earth is even more poorly constrained as the atmospheric composition at that time is not well known.

Hydrogen isotope (D/H) ratio has been used to constrain the global cycle and loss of water on Earth, as it fractionates through planetary processes. Earth's mantle is known to have $\delta D = -80\text{‰}$ to -60‰ ($\delta D = [(D/H)_{sample}/(D/H)_{reference} - 1] \times 10^3$, where the reference is the standard mean ocean water, hereafter SMOW), which is lower than that of today's oceans (defined here as the total hydrosphere) (Kyser and O'Neil, 1984; Clog et al., 2013). The low mantle δD value has been considered to suggest that the mantle became isolated from the oceans through geologic time (Kyser and O'Neil, 1984), or that water in the mantle has been isotopically fractionated from the source seawater because of seafloor alteration and slab dehydration processes (Lécuyer et al., 1998; Shaw et al., 2008, 2012). Isotopic analysis of Archean minerals and rocks has found that Archean seawater has a δD value lower than that of present-day oceans, which has been interpreted as a signature of water loss caused by the hydrogen escape (Hren et al., 2009; Pope et al., 2012).

While D/H ratio has been widely utilized to constrain those processes of the water cycle and loss, there is no comprehensive model of the D/H evolution which involves all relevant processes. Previous studies considered the degassing and regassing (Lécuyer et al., 1998; Shaw et al., 2008) or the hydrogen escape (Pope et al., 2012) only. In addition, the D/H ratios of the mantle and Archean seawater have been considered separately to constrain these different processes. Because all water reservoirs are coupled to each other, all these processes and D/H constraints should be considered simultaneously, which is the aim of this study.

We model the global water cycle taking seafloor hydrothermal alteration, chemical alteration of continental crust, slab subduction, atmospheric escape, and degassing at mid-ocean ridges, hot spots, and arcs into account. The model calculations are compared with the D/H ratios of water in different reservoirs on present-day Earth and of Archean seawater to constrain the rates of hydrogen escape from early Earth and of secular regassing on present-day Earth. Section 2 presents the model. Section 3 shows the results. The implications for the evolution of water on Earth are discussed in Section 4. We conclude in Section 5.

2. Methods

2.1. Model

We constructed a global water cycle model taking the D/H compositions into account. Four reservoirs were considered in our model: the oceans, continental crust, oceanic crust, and mantle. These reservoirs exchange water through seafloor hydrothermal alteration, chemical alteration of continents, slab subduction, and degassing at mid-ocean ridges, hot spots, and arcs (Fig. 1). Hydrogen loss to space induced by photolysis of methane was considered to have occurred on early Earth before the GOE at 2.5 Ga. The oceans in our model include water in small reservoirs that exchange water with oceans over short timescales: atmosphere, biosphere, surface water, ground water, and glaciers/polar ice, see Table 2. Hereafter the oceans with the small reservoirs are referred to as "bulk oceans" when we would like to distinguish them from seawater without small reservoirs. Exploring the possible ranges of
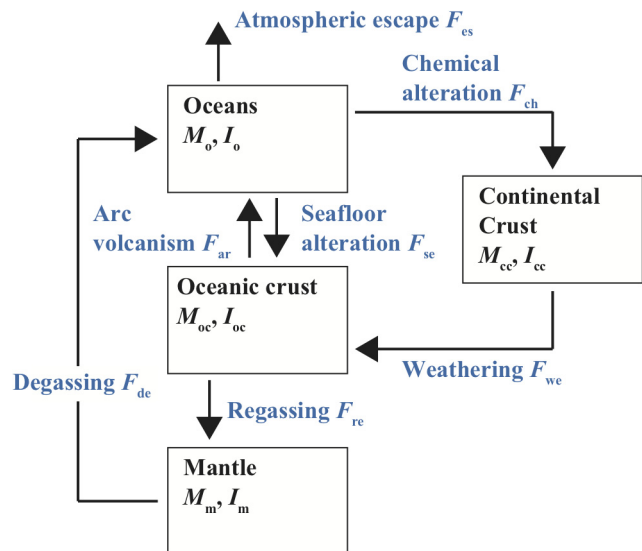
Fig. 1. Schematic view of Earth's water cycle in our model.

fluxes, we constrain the water cycle and discuss the implications for the evolution of water on Earth.

Evolution of the masses and D/H ratios of water in each reservoir was calculated by using the following equations,

$$\frac{dM_i}{dt} = \sum_{sources} F_k - \sum_{sinks} F_k \tag{1}$$

$$\frac{d}{dt}(M_i I_i) = \sum_{sources} F_k f_k I_{i'} - \sum_{sinks} F_k f_k I_i \tag{2}$$

$$\frac{f_{re}}{f_{ar}} = f_{dehy} \tag{3}$$

$$\frac{F_{ar}}{F_{ar} + F_{re}} f_{ar} + \frac{F_{re}}{F_{ar} + F_{re}} f_{re} = 1 \tag{4}$$

where M_i and I_i are the mass and D/H ratio of water in the reservoir i, and F_k and f_k are the flux of the process k and its fractionation factor. The sources and sinks for each reservoir are described in Fig. 1. Hereafter subscripts i = o, cc, oc, and m denote the oceans, continental crust, oceanic crust, and mantle, respectively. The subscript i′ in Equation (2) denotes a reservoir other than i. Subscripts k = ch, ar, se, de, es, we, and re denote the chemical alteration, arc volcanism, seafloor alteration, degassing, atmospheric escape, weathering, and regassing, respectively. Equations (3) and (4) give f_{ar} and f_{de} by considering the dehydration-induced fractionation and mass balance. Assuming $d/dt = 0$ in Equation (2) gives a steady state in D/H, which is useful to understand the numerical results (Appendix A).

Our model assumed that the fluxes depend on the masses of water in the reservoirs and time as follows:

$$F_{ch} = F_{ch}^0 \frac{A_c(t)}{A_c^0} \tag{5}$$

$$F_{se} = F_{se}^0 \times f(t) \tag{6}$$

$$F_{ar} = F_{ar}^0 \frac{M_{oc}(t)}{M_{oc}^0} \times f(t) \tag{7}$$

$$F_{de} = F_{de}^0 \frac{M_m(t)}{M_m^0} \times f(t)^{\frac{1}{2}} \tag{8}$$

$$F_{we} = F_{we}^0 \frac{M_{cc}(t)}{M_{cc}^0} \tag{9}$$

$$F_{re} = F_{re}^0 \frac{M_{oc}(t)}{M_{oc}^0} \times f(t) \tag{10}$$

where superscript 0 denotes the reference (present-day) values, A_c is the continental area, and $f(t)$ is the speed of plate tectonics scaled to that on present-day Earth, which accounts for the change of mantle-convection speed due to the cooling suggested by conventional thermal-evolution models (e.g., Stevenson et al., 1983; Höning and Spohn, 2016). The difference in the dependence on $f(t)$ between Equations (6), (7), (10) and (8) originates from the boundary-layer model (Höning and Spohn, 2016).

The continental area A_c as a function of time is given by (McLennan and Taylor, 1982),

$$\frac{A_c}{A_c^0} = \begin{cases} 0.1875 \times \left(\frac{t}{\text{Gyr}}\right) & (t < 0.8 \text{ Gyr}) \\ 0.15 + 0.929 \times \left(\frac{t}{\text{Gyr}} - 0.8\right) & (0.8 \text{ Gyr} < t < 1.5 \text{ Gyr}) \\ 0.8 + 0.0667 \times \left(\frac{t}{\text{Gyr}} - 1.5\right) & (1.5 \text{ Gyr} < t) \end{cases}$$

(11)

We note that, though the evolution of the continental coverage is controversial, our results are shown to depend only weakly on the choice of the continental growth model (subsection 4.7).

The plate speed scaled by the present-day value $f(t)$ is given by,

$$f(t) = 10^{-(t/4.5 \text{ Gyr} - 1)}$$

(12)

Equation (12) reflects the model of Höning and Spohn (2016), which argued that the speed of subduction was ∼2–10 times faster when the potential temperature of the mantle was ∼100–300 K hotter than today (Herzberg et al., 2010). In contrast, a recent model based on the energetics of plate-tectonic mantle convection proposed that the tectonic speed and surface heat flux have been nearly constant throughout Earth's history (Korenaga, 2003; Korenaga et al., 2017), which implies $f(t) = 1$. We considered both the former and latter cases. Hereafter the two thermal evolution models are referred to as the faster and slower plate tectonics (PT) models, respectively. Models assuming time-independent (constant) fluxes were also explored to show the basic properties of the evolution of D/H (Appendix B).

2.2. Parameters

Our assumptions on parameters are summarized in Table 1 (Supplementary text S1). We assumed $M_o^0 = 1$ ocean, $M_{cc}^0 = 0.2$ oceans, and $M_{oc}^0 = 0.1$ oceans (1 ocean = 1.4×10^{21} kg). Most of our models assumed $M_m^0 = 1$ ocean, but some models showed the integrated regassing to be larger than 1 ocean. In these cases, we increased M_m^0 iteratively until the model results in M_m at present which agrees with the assumed M_m^0.

The present-day net-regassing flux $F_{re,net}$ ($= F_{re}^0 - F_{de}^0$) and escape flux before 2.5 Ga F_{es} are treated as independent parameters. We assumed $F_{de}^0 = 1.0 \times 10^{11}$ kg/yr, $F_{se}^0 = 10 \times 10^{11}$ kg/yr, $F_{ch}^0 = 1.5 \times 10^{11}$ kg/yr, $F_{we}^0 = 1.0 \times 10^{11}$ kg/yr, $F_{re}^0 = F_{de}^0 + F_{re,net}^0$, and $F_{ar}^0 = F_{se}^0 + F_{we}^0 - F_{re}^0$, respectively (Supplementary text S2). Models assuming different values of the fluxes were also explored to show the basic behavior of the system (Appendix B).

Our standard model assumed the values of fractionation factors as summarized in Table 1. Considering the uncertainty of fractionation factors (Supplementary text S3), we also examined the cases where different values were assumed.

While our model assumed that the majority of Earth's water had been delivered before the solidification of magma oceans, part of water might have been delivered by the late accretion of comets. In order to investigate the influence of the possible late accretion of comets, we also explored models where the cometary delivery was implemented by an input of 0.01 ocean water with $\delta D = 1000‰$ at 4.1 Ga (Supplementary text S5).

Table 1

Summary of parameters and initial conditions (see Supplementary text S1–4 for references). 1 ocean = 1.4×10^{21} kg. An apostrophe denotes the fractionation from the water in oceans before the correction by adding small reservoirs (Supplementary text S3).

Present-day water fluxes [10^{11} kg/yr]	
F_{de}^0	1.0
F_{se}^0	10
F_{ch}^0	1.5
F_{we}^0	1.0
F_{re}^0	$F_{de}^0 + F_{re,net}$
F_{ar}^0	$F_{se}^0 + F_{we}^0 - F_{re}^0$
Fractionation factors	
$10^3 \ln f_{de}$	0 (standard), 10
$10^3 \ln f_{se}'$	−30
$10^3 \ln f_{ch}'$	−80
$10^3 \ln f_{we}$	0
$10^3 \ln f_{re}$	Equations (3) and (4)
$10^3 \ln f_{ar}$	Equations (3) and (4)
$10^3 \ln f_{dehy}$	−40 (standard), −23
$10^3 \ln f_{es}$	−150
Present-day water masses [ocean]	
M_o^0	1
M_{cc}^0	0.2
M_{oc}^0	0.1
M_m^0	1 or >1
Initial water masses	
M_o^i	$M_o^0 + M_{cc}^0 + M_{es} + M_{re}$
M_{cc}^i	0 ocean
M_{oc}^i	M_{oc}^0
M_m^i	$M_m^0 - M_{re}$

2.3. Initial conditions

The initial conditions of water volumes were assumed as follows (Table 1 and Supplementary text S4). Because there was no continental crust initially (Equation (11)), $M_{cc}^i = 0$ oceans was assumed. The water in sediments on present-day Earth was assumed to be initially partitioned into the oceans. We further assumed that the integrated water lost by escape M_{es} originated from the oceans. Therefore, the initial water in oceans was given by $M_o^i = M_o^0 + M_{cc}^0 + M_{es} + M_{re}$, where M_{re} is the integrated net regassing. The regassed water M_{re} is not given *a priori*, but it was given by iteration. The initial mantle water was given by $M_m^i = M_m^0 - M_{re}$.

We assumed that all the reservoirs have the same δD and iteratively change the value to obtain the present-day oceanic δD value which equals the SMOW (Supplementary text S4). We note that the initial δD values obtained by this procedure were within the range of carbonaceous chondrites: $\delta D = -200‰$ to 300‰ (Lécuyer et al., 1998).

2.4. Constraints from D/H

Models are considered successful if they satisfy the constraints on the D/H ratios of present-day reservoirs (Table 2) and of the Archean seawater. Present-day Earth's seawater have $\delta D = 0‰$ by definition. Summing up water in oceans and small reservoirs (atmosphere, biosphere, surface water, groundwater, and glaciers) leads to the bulk oceanic $\delta D = -12‰$ to $-7.1‰$. The gap from SMOW mostly originated from the contribution of low δD glaciers and polar ice. Sedimentary rocks on continental crust and metamorphic rocks on oceanic crust have $\delta D = -100‰$ to $-60‰$

Table 2

Sizes and D/H ratios of water reservoirs on present-day Earth. 1 ocean = 1.4×10^{21} kg.

Reservoir	Amount of water (ocean)	δD (‰)
Oceans (including small reservoirs)	1.0	−12 to −7.1
Oceans	0.98[a]	0[a]
Atmosphere	9.3×10^{-6} [a]	−70 to +10[b]
Biosphere	3.4×10^{-5} [a]	−130 to −70[c]
Surface water	1.5×10^{-4} [a]	−300 to +10[d]
Ground water	7.5×10^{-3} [a]	−300 to +10[d]
Glaciers/Polar ice	2.4×10^{-2} [a]	−400 to −300[c]
Oceanic crust	0.10[a]	−50 to −30[f]
Continental crust	0.20[a]	−100 to −60[c]
Mantle	1.0[e]	−80 to −60[g]

[a] Bodnar et al. (2013) and references therein.
[b] "Volumetrically most important meteoric waters" from Sheppard (1986).
[c] Lécuyer et al. (1998) and references therein.
[d] Pope et al. (2012) and references therein.
[e] Korenaga et al. (2017) and references therein.
[f] Lécuyer et al. (1998); Shaw et al. (2008) and references therein.
[g] Kyser and O'Neil (1984); Clog et al. (2013).

and $\delta D = -50$‰ to −30‰, respectively (Lécuyer et al., 1998; Shaw et al., 2008). Earth's mantle has $\delta D = -80$‰ to −60‰ (Kyser and O'Neil, 1984; Clog et al., 2013).

The D/H ratio of paleo-seawater has been estimated from isotopic analysis of minerals and rocks which interacted with seawater (Wenner and Taylor, 1974; Lécuyer et al., 1996; Kyser et al., 1999; Hren et al., 2009; Pope et al., 2012). We adopted $\delta D = -25 \pm 5$‰ proposed by Pope et al. (2012) as the constraint on 3.8 Ga seawater, because they have derived this value by combining hydrogen and oxygen isotope measurements of serpentine samples, in which primitive isotopic signatures have been well preserved. We will discuss other data sets in subsection 4.4. We assumed that the range of δD values between those of the bulk ocean and the ocean (seawater) should match the evaluated δD of the Archean seawater. Assuming constant $\ln f'$ corresponds to the case where the mass ratio of glaciers/polar ice to bulk oceans has been constant through time. Because there is no evidence of glaciation before approximately 2.9 Ga (Young et al., 1998), considering the range of δD is a conservative assumption.

3. Results

The ranges of $F_{\text{re,net}}$ and F_{es} where the constraints on present-day and Archean D/H were satisfied are shown for the slower and faster PT models in Figs. 2a and 2b, respectively. The standard model was assumed for fractionation factors. The initial water mass in the oceans M_o^i is also shown. We calculated the evolution of masses and D/H ratios of the water reservoirs for each set of $F_{\text{re,net}}$ and F_{es}. Examples of evolutionary tracks are shown in Figs. 3 and 4. The results for different values of fractionation factors are shown in Fig. 5. The influence of the possible late accretion of comets are considered in Fig. 6. As explained below, the results showed that the slower PT model assuming $F_{\text{re,net}} = 0$ and $F_{\text{es}} = 0$ does not satisfy the constraints on D/H (Fig. 2a). Therefore, hydrogen escape from the reduced early atmosphere, secular net regassing (Fig. 2a), or faster plate tectonics on early Earth (Fig. 2b) is required.

3.1. The slower PT model

The evolution of δD_i and M_i (where i is an arbitrary reservoir) in the slower PT model assuming $F_{\text{re,net}} = 0$ and $F_{\text{es}} = 0$ is shown in Fig. 3a. The oceanic δD_o increased through time because of the isotopic fractionation from seafloor alteration, slab dehydration, and chemical alteration of continents. All of these processes
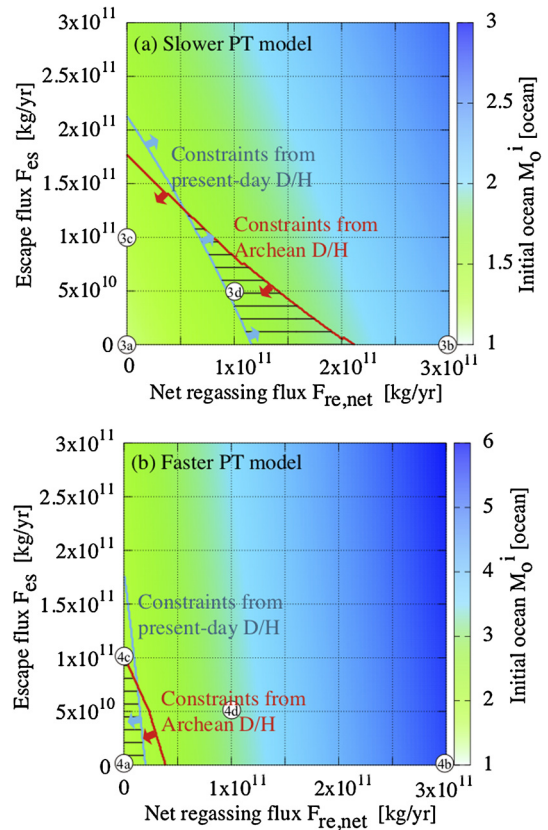
Fig. 2. Range of $F_{\text{res,net}}$ and F_{es} where the constraints on D/H are satisfied (the hatched areas). Results for (a) slower plate tectonics (PT) model and (b) faster PT model are shown. The present-day D/H ratios of the water reservoirs were reproduced above and below the sky-blue line for (a) and (b), respectively. The D/H of the Archean seawater was reproduced below the red line. Color contour denotes M_o^i. Marks in figures correspond to the parameter sets shown in Figs. 3 and 4. (For interpretation of the colors in the figure(s), the reader is referred to the web version of this article.)

led to D-enrichment in liquid water. The water in the oceans M_o decreased in response to the increase of the water in sediments M_{cc} because continental growth promoted chemical alteration. The mantle δD_m decreased through time because of the subduction of deuterium-poor water as hydrous minerals. The continental crust δD_{cc} increased through time following the increase of the oceanic δD_o. The oceanic crust δD_{oc} initially decreased because of the isotopic fractionation by seafloor alteration and then increased in the latter period time following the increase of the oceanic δD_o. The integrated increase in δD_o caused by the deep water cycle and continental growth reached $\sim +20$‰, which is enough to reproduce the increase of δD_o from the low δD Archean seawater (Pope et al., 2012). However, the present-day δD_m in the model disagreed with the value inferred from sample analyses (Kyser and O'Neil, 1984; Clog et al., 2013). The deep water cycle in our model evolved toward a steady state given by $\Delta D_{o-m} \equiv \delta D_o - \delta D_m \sim 70$‰, which is consistent with ΔD_{o-m} of the present-day Earth (Appendix A and Appendix B), but the rates of degassing and regassing are too small to reach the steady state within 4.5 Gyr. The constraints on the continental crust δD_{cc} and oceanic crust δD_{oc} were satisfied in all cases because both δD_{cc} and δD_{oc} are in a steady state with the oceanic δD_o (Appendix A).

Secular net regassing and hydrogen escape can increase ΔD_{o-m} (Figs. 3b and 3c). The secular regassing transported deuterium-poor water from the oceans to mantle and the hydrogen escape removed deuterium-poor water from the oceans (more precisely, from the atmosphere, which exchanges water with the oceans). The net regassing on present-day Earth in the slower PT model
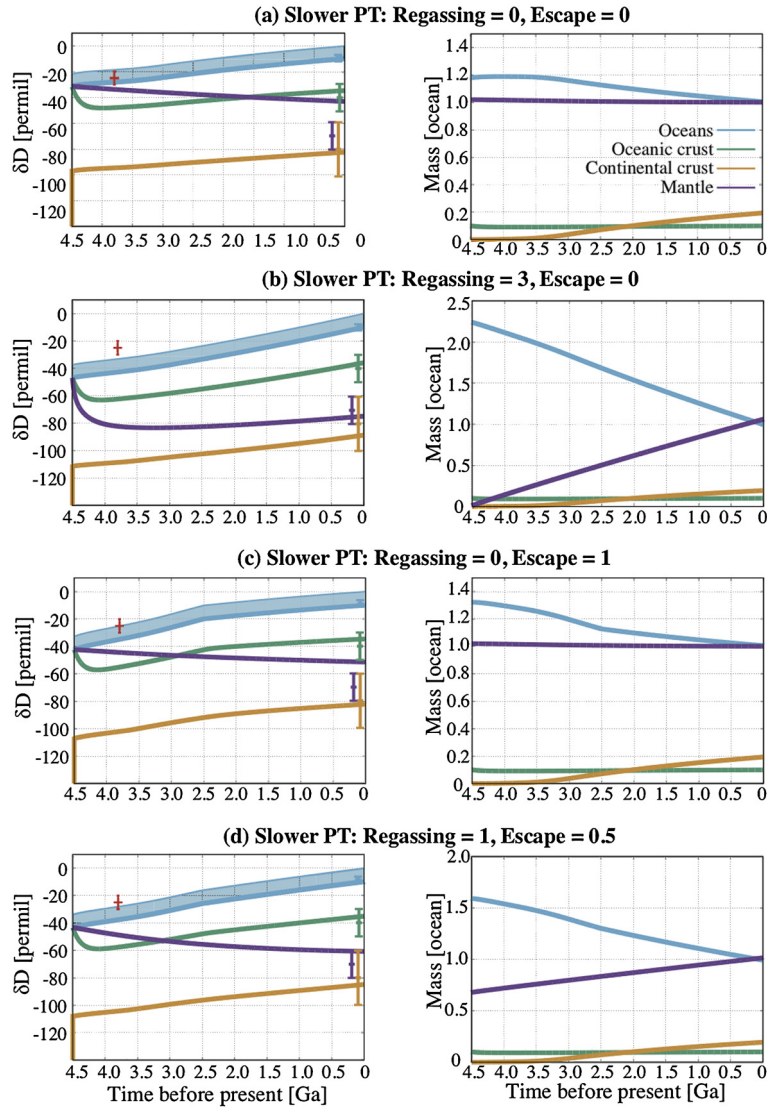
Fig. 3. Time evolution of the points labeled 3a–d from the slower PT models in Fig. 2a. Left: δD of oceans (thin cyan lines), bulk oceans (thick cyan lines), oceanic crust (green lines), continental crust (yellow lines), and mantle (purple lines) as a function of time. Data points are δD values of reservoirs on present-day Earth (subsection 2.4 and Table 2) and 3.8 Ga seawater (Pope et al., 2012). The shaded range denotes the possible range of oceanic δD (see subsection 2.4). Right: masses of water in bulk oceans (cyan lines), oceanic crust (green lines), continental crust (yellow lines), and mantle (purple lines) as a function of time.

led to steady decrease and increase in M_o and M_m, respectively (Fig. 3b). The mantle δD_m started to increase at ∼3.5 Ga following the increase of the oceanic δD_o. The hydrogen escape removed water from the oceans M_o before the GOE at 2.5 Ga (Fig. 3c). In contrast to the secular regassing (Fig. 3b), the hydrogen escape and its cessation at 2.5 Ga resulted in the kink in the evolution of δD_o (and consequently, in that of δD_{cc} and δD_{oc}) at 2.5 Ga. The coexistence of the secular regassing diminishes the kink caused by the cessation of hydrogen escape, depending on $F_{re,net}$ and F_{es} (Fig. 3d).

A comparison of the results in the slower PT models with the D/H constraints allowed us to constrain $F_{re,net}$ and F_{es} (Fig. 2a). Because the change in δD values was too small to reproduce present-day ΔD_{o-m} in the model assuming $F_{re,net} = 0$ and $F_{es} = 0$ (Fig. 3a), this provided a lower limit on $F_{re,net}$ and F_{es} that can satisfy the constraint on present-day D/H (the sky-blue line in Fig. 2a). We note that there was also a upper limit in these values above which ΔD_{o-m} was too large as seen in Fig. 2b, but it was outside the range of Fig. 2a. On the other hand, the increase in the oceanic δD_o inferred from the low δD of the Archean seawater (Pope et al., 2012) was reproduced in the model assuming

$F_{re,net} = 0$ and $F_{es} = 0$ (Fig. 3a). Because both the secular regassing and hydrogen escape promote the increase in δD_o, there was an upper limit on $F_{re,net}$ and F_{es} to satisfy the constraint on the Archean seawater (the red line in Fig. 2a). All the constraints on D/H were satisfied in the limited range of $F_{re,net}$ and F_{es} (the hatched area in Fig. 2a).

The range of $F_{re,net}$ and F_{es} depends on the assumed values of fractionation factors. Within the range of uncertainties (Table 1), assuming smaller fractionation for dehydration led to the hatched area moving to the right (Fig. 5a), whereas assuming larger fractionation for degassing led to the hatched area moving to the left (Fig. 5c).

The possible late accretion of comets moderately influences the resulting range of $F_{re,net}$ and F_{es}, but the D/H constrains still require at least either one of the two mechanisms: secular net regassing or hydrogen escape (Fig. 6a). Because comets have a high D/H ratio, the input resulted in an increase in δD_o (Fig. 6b), while its contribution to Earth's water budget (∼ 0.01 ocean water, Supplementary text S5) is negligible. The input of D-enriched water decreased $F_{re,net}$ and F_{es} required to reproduce the present-day
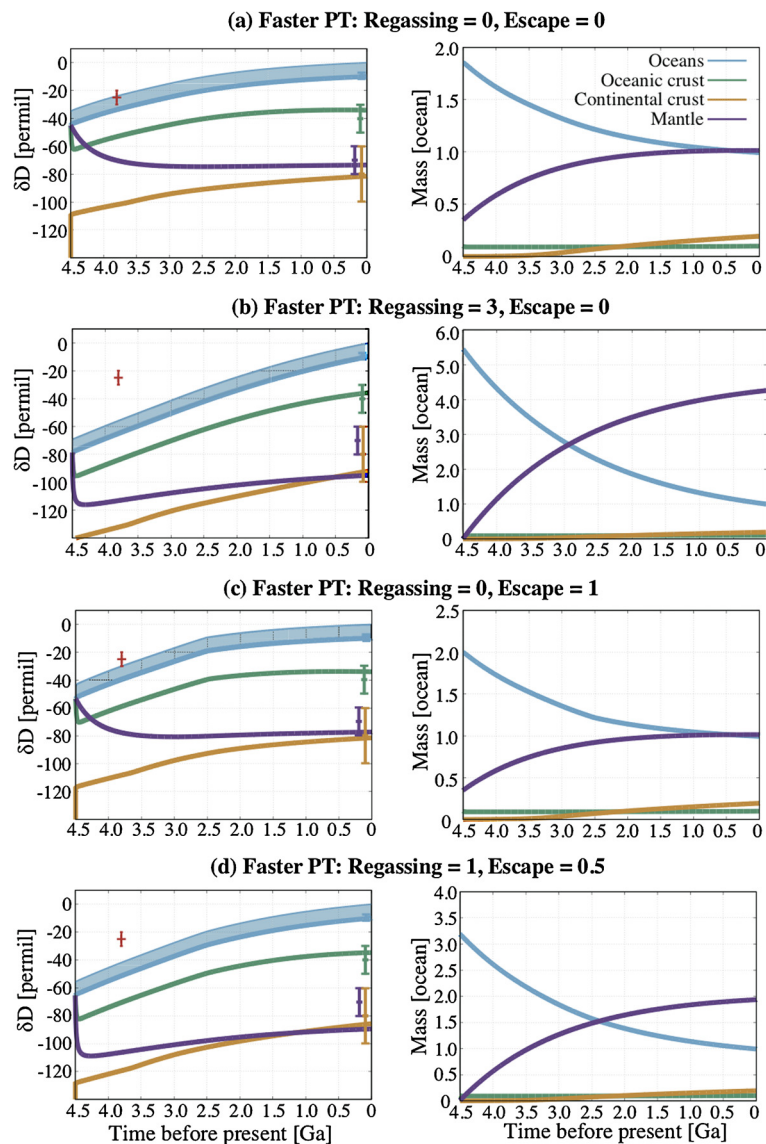
Fig. 4. The same as Fig. 3, but the time evolution for the points labeled 4a–d from the faster PT models in Fig. 2b are shown.

D/H ratios and increased these fluxes required to reproduce the D/H ratio of the Archean seawater.

3.2. The faster PT model

In contrast to the slower PT model assuming $F_{re,net} = 0$ and $F_{es} = 0$ (Fig. 3a), the efficient water cycle on early Earth in the faster PT model led to the δD values nearly reaching steady state in ΔD_{o-m} (Appendix A) even assuming $F_{re,net} = 0$ and $F_{es} = 0$ (Fig. 4a). As with the slower PT model, the isotopic fractionation resulted from the seafloor alteration, slab dehydration, and chemical alteration of continents. The faster PT model assuming the secular regassing showed a continuous increase in both the oceanic δD_o and mantle δD_m (Fig. 4b), which is qualitatively the same as the slower PT model (Fig. 3b), but the change is larger because of the higher regassing rate in the past. Though the hydrogen escape had a minor influence on the evolution of the water masses in the reservoirs, its effect on the evolution of D/H was more pronounced (Figs. 4c and 4d) because of the efficient fractionation by hydrogen escape compared to the other processes (Table 1).

The faster PT models assuming $F_{re,net} = 0$ and $F_{es} = 0$ satisfied both the constraints from D/H of the present-day water reservoirs and of the Archean seawater (Fig. 2b). Because assuming the secular regassing or hydrogen escape increased the change in δD_o and the present-day ΔD_{o-m} (Fig. 4), both the constraints on present-day and Archean D/H gave an upper limit on $F_{re,net}$ and F_{es} (the purple and red lines in Fig. 2b, respectively). Neither the secular regassing nor hydrogen escape is necessarily required and the allowed range of $F_{re,net}$ and F_{es} was smaller than that in the slower PT model.

Changing the values of fractionation factors in the faster PT model showed a similar behavior to the slower PT model (Figs. 5b and 5d), but the key result—neither the secular regassing nor hydrogen escape is necessarily required in the faster PT model—does not change.

Assuming cometary input slightly changed the range of $F_{re,net}$ and F_{es} allowed to reproduce D/H constraints (Fig. 6c). The input of D-enriched water (Fig. 6d) decreased $F_{re,net}$ and F_{es} allowed to reproduce the present-day D/H ratios and increased these fluxes allowed to reproduce the D/H ratio of Archean seawater. Again, the results showed that neither the secular regassing nor hydrogen escape is necessarily required in the faster PT model.

Compared to the slower PT models (Figs. 2a and 3), the faster PT models resulted in a large decrease in the oceanic volume
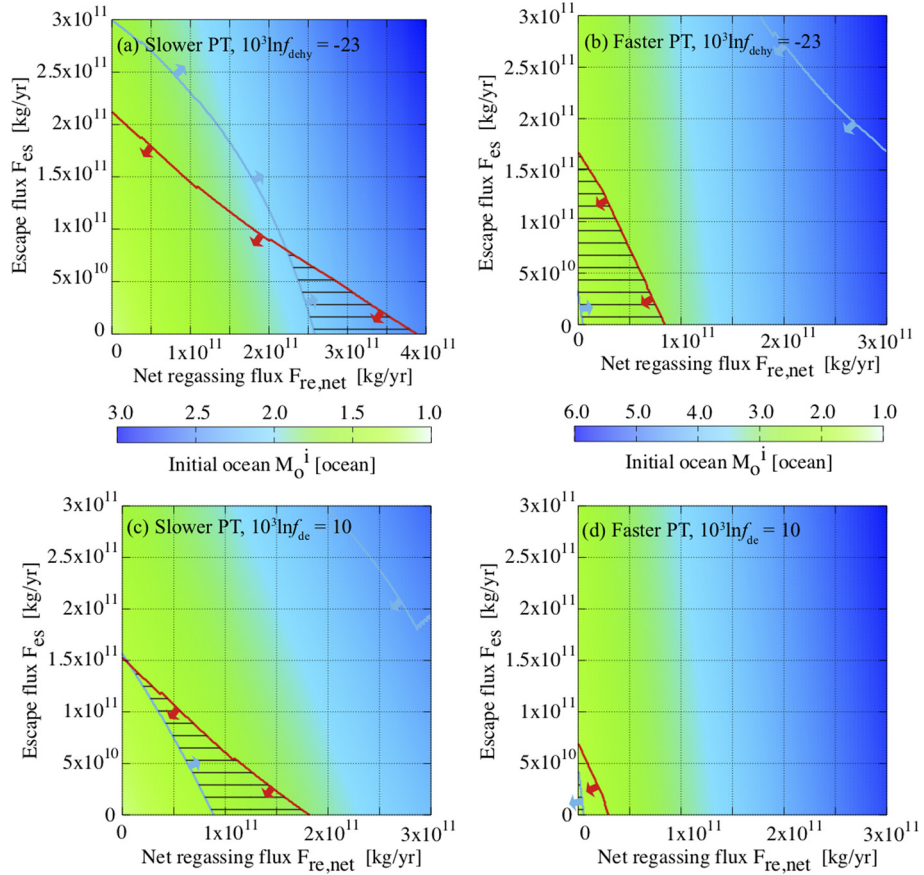
Fig. 5. The same as Fig. 2, but different values of fractionation factors are assumed (Table 1). The cases for (a, b) $10^3 \ln f_{dehy} = -23$ and (c, d) $10^3 \ln f_{de} = 10$ are shown.
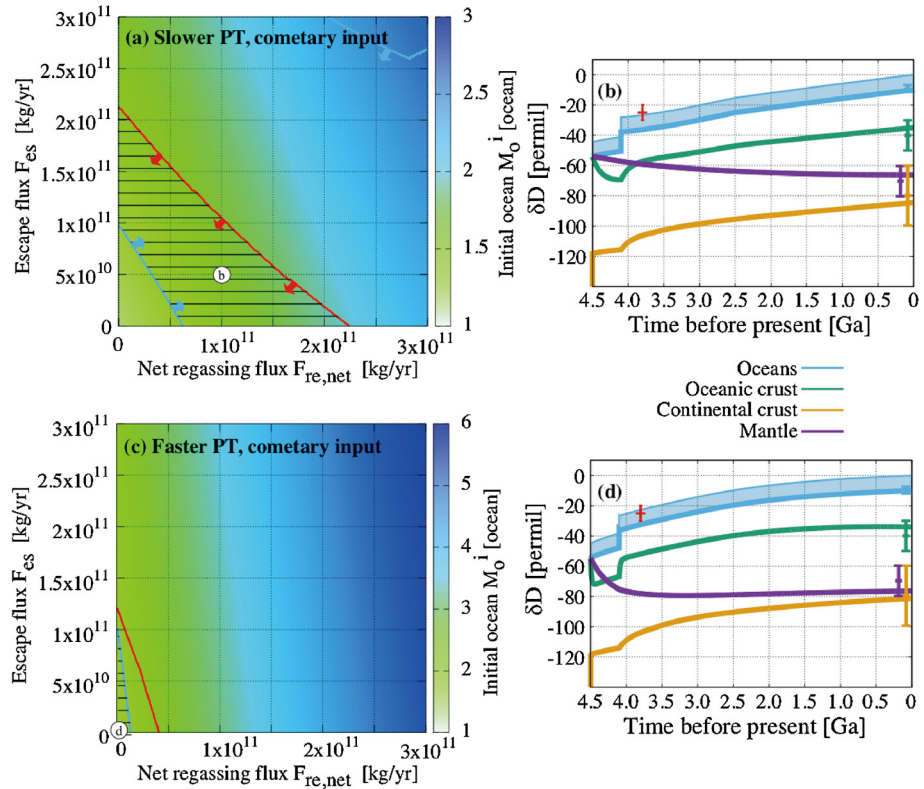
Fig. 6. The same as Fig. 2, but cometary input was assumed at 4.1 Ga (see text).

(Figs. 2b and 4). In the faster PT models, different dependence on the thermal evolution is assumed for the regassing (Equation (10)) and degassing (Equation (8)) as predicted by the boundary-layer model of the thermal evolution (Höning and Spohn, 2016). The difference resulted in the net regassing being larger in the earlier period. Even in the case where the balance was assumed for the present-day Earth ($F_{re,net} = 0$), ~0.7 oceans of water subducted in 4.5 Gyr (Fig. 4a). The faster PT models assuming the net regassing today showed much higher regassing in the past, leading to ~4.3 oceans of water subducted throughout Earth's history (Fig. 4b).

4. Discussion

4.1. Evolution of water on Earth constrained by D/H

The evolution of water on Earth can be constrained by comparing our results with the D/H ratios of present-day water reservoirs (subsection 2.4 and Table 2). The differences in δD between the present-day oceans, continental and oceanic crust, and mantle were shown to result from isotopic fractionation through the seafloor alteration, slab dehydration, and chemical alteration (Section 3). The D/H ratios of present-day reservoirs can be understood by using the steady state (Appendix A and Appendix B). We note that a steady state in hydrogen isotope compositions of the oceans and mantle has been proposed by previous studies (Taylor, 1974; Javoy, 2005), though dehydration-induced fractionation has not been considered in them. However, the model also showed that the rates of present-day regassing and degassing are small so that the system does not reach the present-day ΔD_{o-m} within 4.5 Gyr (Fig. 3a). Therefore, the hydrogen escape from the reduced early atmosphere, secular regassing, or faster plate tectonics on early Earth was needed to explain the present-day state of D/H ratios in the reservoirs (Fig. 2).

The low δD of Archean seawater (Pope et al., 2012) further constrains the evolution of water on Earth (subsection 2.4). Both the slower and faster PT models assuming $F_{re,net} = 0$ and $F_{es} = 0$ resulted in the secular increase in the oceanic δD_o as a result of the deep water cycle and continental growth, which agreed with the constraint on the Archean seawater (Figs. 3a and 4a). Because the secular regassing and hydrogen escape promote the increase in δD_o, the constraint on δD of the Archean seawater gave an upper limit on $F_{re,net}$ and F_{es} (Fig. 2).

These three possibilities—the hydrogen escape, faster plate tectonics on early Earth, and secular regassing—are mutually exclusive. For instance, in our standard model, the slower PT model needed $F_{re,net} = 0.6–2.1 \times 10^{11}$ kg/yr or $F_{es} = 0–1.2 \times 10^{11}$ kg/yr (Fig. 2a). Assuming larger $F_{re,net}$ leads to lower F_{es}, and vice versa. On the other hand, the faster PT model allowed much smaller values: $F_{re,net} = 0–0.2 \times 10^{11}$ kg/yr and $F_{es} = 0–1.0 \times 10^{11}$ kg/yr.

Considering the possible ranges of fractionation factors and late accretion of comets (Figs. 2, 5, and 6) yielded $F_{re,net} < 3.9 \times 10^{11}$ kg/yr and $F_{es} < 2.1 \times 10^{11}$ kg/yr. The upper limit of the present-day regassing rate is higher than the upper limit proposed by Parai and Mukhopadhyay (2012) from the constraint on the sea-level change ($F_{re,net} = 1.0 \times 10^{11}$ kg/yr), but is comparable with the range recently argued by Korenaga et al. (2017) considering the change in buoyancy of continental lithosphere relative to oceanic lithosphere through time: $F_{re,net} = 3.0–4.5 \times 10^{11}$ kg/yr. The upper limit of the rate of water loss due to hydrogen escape $F_{es} = 2.1 \times 10^{11}$ kg/yr corresponds to ~900 ppmv of CH_4 (Equation S1). The high CH_4 concentration might be possible during the early Archean (Kharecha et al., 2005).

The secular regassing, hydrogen escape, and chemical alteration promoted by continental growth contributed to the secular decrease of oceanic water in our model. In the slower PT model, the possible maximum value of M_o^i is given when $F_{re,net} = 3.9 \times$ 10^{11} kg/yr was assumed (Fig. 5a). The initial mass of the bulk oceans was 2.5 oceans (considering 1.3 oceans later subducted and 0.2 oceans formed sediments). In the faster PT model, the possible maximum value of M_o^i is given when $F_{re,net} = 0.83 \times 10^{11}$ kg/yr was assumed (Fig. 5b), the initial mass was 2.9 oceans (1.7 oceans subducted and 0.2 oceans formed sediments). These values are comparable with the estimate of Korenaga et al. (2017) to reconcile the continental freeboard with the geologic constraints.

We suggest that the D/H constraints are consistent with the secular regassing scenario where water in the present-day mantle entirely resulted from the regassing throughout Earth's history. The scenario is consistent not only with the geologic constraints on continental freeboard when the change in relative buoyancy of continental lithosphere is taken into account (Korenaga et al., 2017), but also with the theoretical predictions of crystallization of magma oceans, where the majority of water was partitioned into the atmosphere and oceans (Hamano et al., 2013). Such initial conditions have been argued to be ideal for initiating the plate tectonics (Korenaga, 2013).

4.2. Implications for future analysis of D/H on early Earth

The three scenarios that explain the δD values of the present-day and Archean reservoirs—the hydrogen escape, secular regassing, and faster plate tectonics on early Earth—can be distinguished by future analyses of samples that record the D/H ratios of the seawater *and mantle* on early Earth. The evolution of the oceanic and mantle δD for various sets of $F_{re,net}$ and F_{es} and for the slower and faster PT models is shown in Fig. 7. Though the increase in the oceanic δD_o has been interpreted as a signature of hydrogen escape (Pope et al., 2012), Figs. 7a and 7b showed that the increase is possible without the escape. Instead, the kink at the time of the GOE, if confirmed, would be a signature of hydrogen escape from reduced early atmosphere. Constraining the oceanic δD_o at the time of the GOE would help us to distinguish the scenarios.

While the difference in the oceanic δD_o between the slower and faster PT models is small (Figs. 7a and 7b), the mantle δD_m signal can discriminate between these scenarios (Figs. 7c and 7d). In contrast to the slower PT model where the mantle δD_m decreased continuously, the faster PT model showed a rapid change in the earlier period. Identifying the past mantle δD_m as well as the oceanic δD_o would allow us to distinguish the three scenarios. In addition to the D/H ratios of the oceans and mantle in the Archean, those from the Hadean to the Phanerozoic, if combined with our model, would be useful to constrain the evolutionary scenarios.

4.3. Comparison with previous studies

Earth's deep water cycle and loss by hydrogen escape have been investigated in previous studies by using constraints on D/H. Lécuyer et al. (1998) modeled the deep water cycle considering two reservoirs: the oceans and mantle. They argued that hydrogen isotope variations of the oceans in time may have occurred in response to the imbalance between the rates of regassing and degassing. Their model showed that the system eventually reached a steady state in δD_o. In contrast, our model showed that δD_o kept changing (increasing) in response to the imbalance (regassing) (Section 3). The difference originated from the assumption about the isotopic fractionation: they assumed constant δD values both for regassed and degassed water, whereas we calculated the δD values from the fractionation factors (subsection 2.1). In that regard, the results of our model is more realistic than those of Lécuyer et al. (1998).
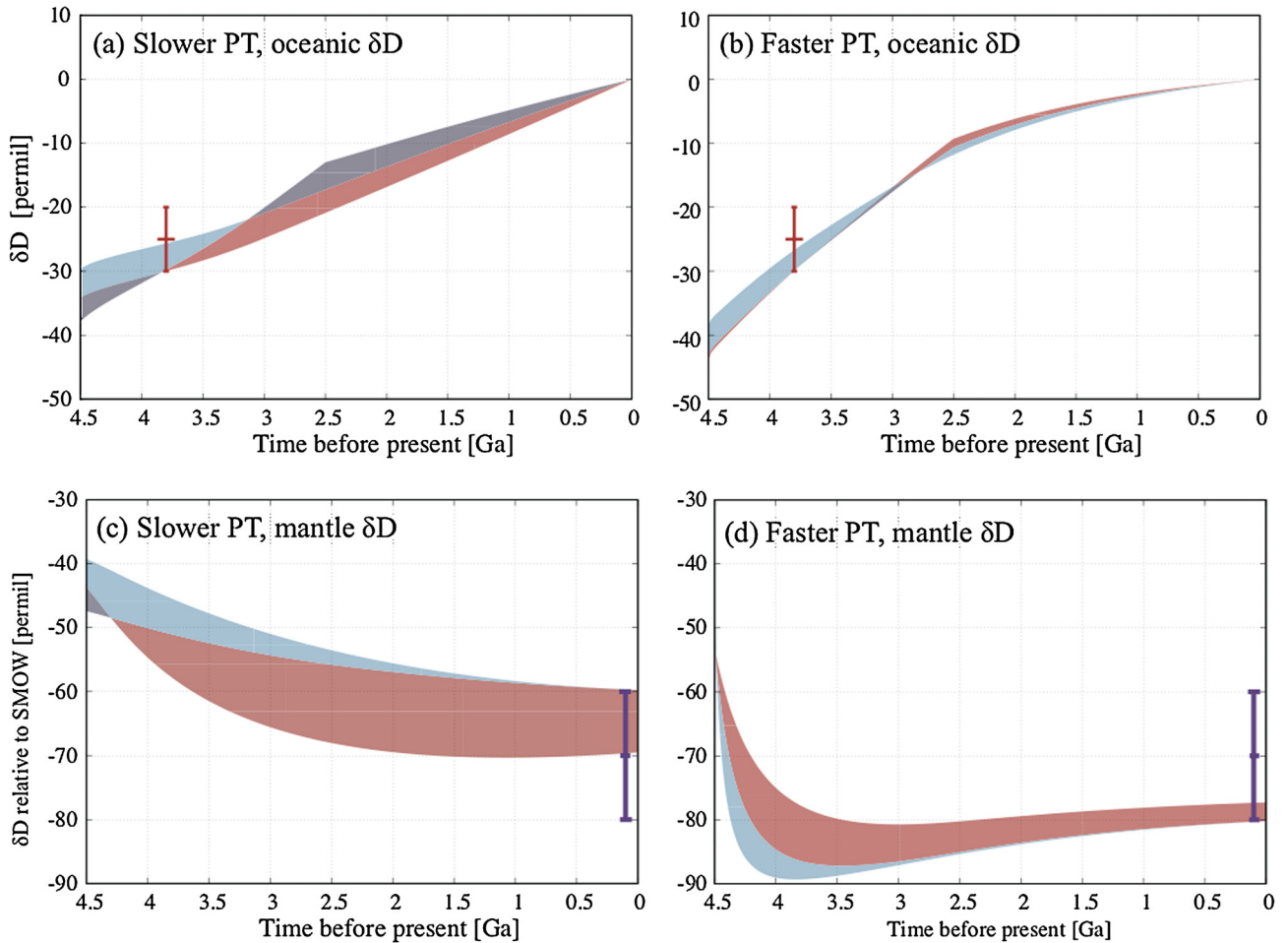
Fig. 7. δD of (a, b) oceans and (c, d) mantle as a function of time. The results for (a, c) the slower and (b, d) faster PT models are shown. Shaded areas show the possible ranges of evolutionary tracks that correspond to the parameter sets in hatched areas in (a, c) Fig. 2a and (b, d) Fig. 2b along the sky-blue and red lines. Colors of the shaded ranges correspond to those of boundary lines in Fig. 2. Data points are δD of Archean seawater and of present-day mantle (the same as Fig. 3).

Shaw et al. (2008) also modeled the long-term water cycle between the oceans and mantle by taking the isotopic fractionation caused by the seafloor alteration and slab dehydration into account. Assuming the net balance between the regassing and degassing, they showed the continuous increase and decrease in δD_o and δD_m, respectively. Their model even resulted in all the deuterium in the system being partitioned into the oceans after the model was integrated for a long enough time. Contrary to Shaw et al. (2008), our model showed that assuming the balance in the fluxes resulted in δD_o and δD_m reaching a steady state determined by the fractionation factors (Appendix B). The difference originated from the treatment of fractionation factor of the seafloor alteration: they defined the fractionation factor as the ratio of the altered MORB D/H to unaltered MORB D/H, while we defined it as the ratio of altered MORB D/H to seawater D/H. Because the water in the hydrous minerals produced by the seafloor alteration originated from seawater, our assumption is more realistic than that of Shaw et al. (2008).

Pope et al. (2012) used mass-balance calculations to derive the amount of water lost by the hydrogen escape based on δD of Archean seawater. They concluded that ∼0.1 oceans of water was lost due to the escape. In contrast, we showed that the lower δD of Archean seawater can be explained by the isotopic fractionation caused by the deep water cycle (seafloor alteration and slab dehydration) and that the hydrogen escape is not necessarily needed (Section 2). The conclusions differ because they neglected the influence of the regassing and degassing on the δD change in the mass-balance calculations. They justified neglecting the contribution of the mantle to the evolution of δD_o by assuming the net balance between the regassing and degassing. However, δD_o changes because of the deep water cycle, even in the case where the net balance was assumed (Appendix B).

4.4. Other data sets of Precambrian seawater D/H

We adopted the D/H ratio of Archean seawater at 3.8 Ga constrained by Pope et al. (2012), but other studies have also estimated the paleo-seawater D/H ratio (Lécuyer et al., 1996; Kyser et al., 1999; Hren et al., 2009). Whereas Pope et al. (2012) have reported $\delta D = -25 \pm 5‰$ and $\delta^{18}O = 2.3‰$ from serpentine samples from 3.8 Ga Isua Supracrustal Belt in West Greenland, Hren et al. (2009) have constrained $\delta D = -70‰$ to $-5‰$ and $\delta^{18}O = -18‰$ to $-8‰$ from 3.4 Ga Buck Reef Chert rocks in South Africa. Also, by assuming $\delta^{18}O = -10‰$ as suggested by a theoretical model (Kasting et al., 2006), Hren et al. (2009) have proposed that the Archean seawater had $\delta D = -60‰$. Reproducing both $\delta D = -25 \pm 5‰$ at 3.8 Ga and $\delta D = -60‰$ at 3.4 Ga in our model is difficult and might require a singular event between the interval. The discrepancy in $\delta^{18}O$ values in the two studies suggests that these data might be incompatible. Because chert has lower concentrations of water than serpentine and the temperature dependence of D/H fractionation between chert and water is not straightforward, Pope et al. (2012) argued that chert is a less well-suited proxy, so that we chose to use Pope et al. (2012)'s data as a reliable anchor in the Archean for the evolution of seawater D/H.

Lécuyer et al. (1996) have proposed $\delta D = 0 \pm 20‰$ from mafic–ultramafic samples from the Chukotat Group of the Lower Proterozoic (2.0–1.9 Ga) Cape Smith fold belt. They have reported the δD values matching closely those found in modern metavolcanic rocks. Kyser et al. (1999) have constrained the D/H ratio of 2.8–2.6 Ga seawater as $\delta D > -20‰$ from serpentine minerals from Archean Abitibi greenstone belt in Ontario. Because the estimates of these earlier studies were less systematic compared to Pope et al. (2012), we did not plot them explicitly. However, these estimates are in accordance with the trend from the δD value of Pope et al. (2012) to that of present-day seawater so that adopting them would hardly change our results quantitatively.

4.5. Subduction regimes

This study investigated the secular evolution of the global water cycle with the numerical modeling under a wide range of parameter spaces (Fig. 2), yet assumed a limited case of cold subduction (Supplementary text S3, $10^3 \ln f_{dehy} = -40$ to -23) where the major water release from the slab to the surface (F_{ar}) occurs mainly due to dehydration of the hydrous minerals of amphibole and lawsonite (Schmidt and Poli, 1998; Maruyama and Okamoto, 2007). However, our model also explored two extreme subduction regimes of faster and slower PT. Subduction velocity along with plate thermal structure and wedge mantle viscosity strongly influences slab surface temperature, which defines the stability of hydrous minerals (Kincaid and Sacks, 1997; Peacock, 1993). Each hydrous mineral may have a different fractionation factor of D/H due to decomposition. In the case of a hot slab, water released by major dehydration events would be in isotopic equilibrium with amphibole ($\sim350\,°C$), epidote and amphibole ($\sim400\,°C$), and chlorite, epidote, and amphibole ($\sim550\,°C$), respectively (Maruyama and Okamoto, 2007). The fractionation factors f_{dehy} of these hydrous minerals range from $10^3 \ln f_{dehy} = -23$ to -48 (Suzuoki and Epstein, 1976; Graham et al., 1984; Chacko et al., 1999). As this range is similar to that in the case of a cold slab, our results would also apply to the case of a hot slab, though the regassing would mainly be contributed to by the cold-slab subduction. The faster PT might have a smaller net regassing flux F_{re} because of the dominance of hot slabs, but our model acknowledged this and involved such uncertainties of F_{re}.

4.6. Onset time of plate tectonics

Our model assumed that plate tectonics has operated since 4.5 Ga, soon after the solidification of magma oceans. The onset time of plate tectonics is controversial, but some studies have suggested that, on the basis of the geochemistry of Hadean zircons, plate tectonics may have already been operating in the Hadean (Harrison, 2009; Korenaga, 2013, and references therein). Korenaga (2013) argued that the ideal initial water distribution to drive plate tectonics is voluminious oceans underlain by a dry mantle. Such conditions were shown to be consistent with the constraints from hydrogen isotopes (subsection 4.1), though our model can apply to other onset times of plate tectonics.

4.7. Uncertainty in the continental growth model

The behavior of our model depended only weakly on the assumed continental growth model. Thus we demonstrate that the evolution of D/H and surface water mass is a poor constraint on continent formation. As sensitivity analysis, we compared the results using the continental growth models of McLennan and Taylor (1982) (Fig. 2) and Armstrong (1981) (Fig. S1) where the continental coverage increased linearly in the first 1 Gyr and kept a constant value. We found that the dependence of the results on the uncertainty in the continental growth model is small compared to that on the uncertainty in the fractionation factors (Fig. 5).

5. Conclusions

We modeled the evolution of the masses and D/H ratios of water in the oceans, continental and oceanic crust, and mantle. The model considered water transport and hydrogen isotopic fractionation by seafloor hydrothermal alteration, chemical alteration of continental crust, slab subduction, hydrogen escape, and degassing at mid-ocean ridges, hot spots, and arcs. The differences in D/H ratios between the present-day oceans, oceanic and continental crust, and mantle were shown to result from isotopic fractionation by seafloor alteration, slab dehydration, and chemical weathering. The current degassing and regassing rates were too small to reach the present-day D/H, so an additional mechanism was required. We showed three evolutionary scenarios that can account for the present-day D/H ratios: (a) hydrogen escape from a reduced early atmosphere, (b) secular net regassing, and (c) faster plate tectonics on early Earth expected from conventional thermal evolution models. A low D/H ratio of Archean seawater at 3.8 Ga has been interpreted as a signature of the hydrogen escape from a reduced early atmosphere. However, our model showed that the secular net regassing throughout Earth's history or faster plate tectonics on early Earth can also reproduce the constraints on D/H. These three scenarios are mutually exclusive. The rates of hydrogen escape from early Earth and secular regassing on present-day Earth are constrained to be lower than 2.1×10^{11} kg/yr and 3.9×10^{11} kg/yr, respectively. The initial oceans could be 2–3 times as voluminous as that on current Earth in the secular regassing scenario. A signature of hydrogen escape before the GOE is visible as a kink in the slope of the evolution of the oceanic D/H ratio. The mantle D/H ratio in the faster plate tectonics model decreased only during the earlier period, whereas the slower plate tectonics model predicted the mantle D/H ratio has been continuously decreasing throughout Earth's history. Therefore, we emphasize the importance of measurements to constrain mantle D/H ratio throughout Earth's history, in addition to that of seawater at the time of the GOE, to distinguish these three evolutionary scenarios.

Appendix A. Derivation of a steady state in D/H

The evolution of δD values of reservoirs can be understood as the change toward a steady state. From Equation (2), the steady state is given by,

$$\frac{I_o}{I_m} = \frac{F_{de} f_{de}}{F_{re} f_{re}} \frac{F_{re} f_{re} + F_{ar} f_{ar}}{F_{se} f_{se} + F_{ch} f_{ch}} \tag{A.1}$$

$$\frac{I_{cc}}{I_o} = \frac{F_{ch} f_{ch}}{F_{we} f_{we}} \tag{A.2}$$

$$\frac{I_{oc}}{I_o} = \frac{F_{se} f_{se} + F_{ch} f_{ch}}{F_{re} f_{re} + F_{ar} f_{ar}}. \tag{A.3}$$

For the parameter values used in our study (Table 1) where water in oceanic crust mostly degassed through arc volcanism, $F_{ar} \gg F_{re}$,
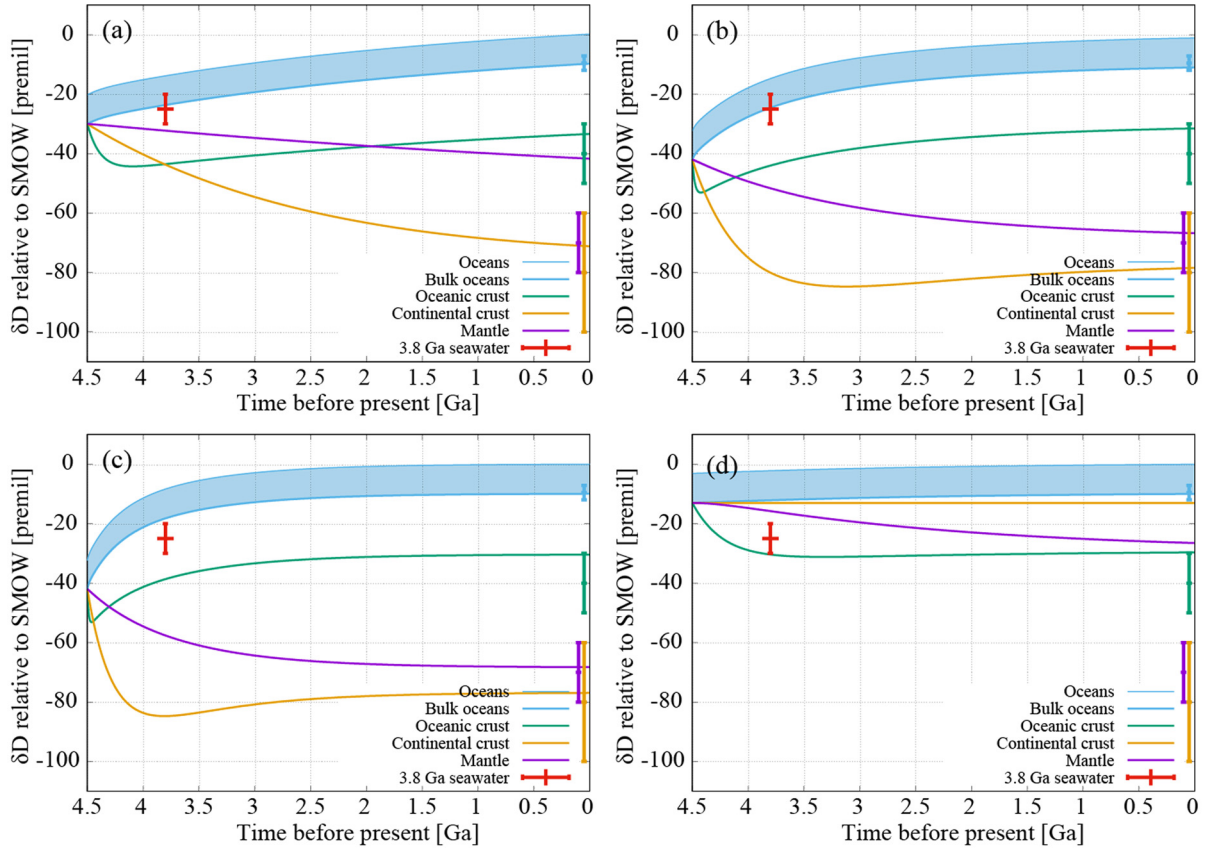
Fig. 8. δD of oceans (thin cyan lines), bulk oceans (thick cyan lines), oceanic crust (green lines), continental crust (yellow lines), and mantle (purple lines) as a function of time in the constant-flux model (see text). The shaded range denotes the possible range of oceanic δD (see subsection 2.4). Results for the dehydration model (a: $F_{de} = 1 \times 10^{11}$ kg/yr, b: $F_{de} = 5 \times 10^{11}$ kg/yr, and c: $F_{de} = 10 \times 10^{11}$ kg/yr) and the non-dehydration model (d: $F_{de} = 5 \times 10^{11}$ kg/yr) are shown. Data points are δD values of reservoirs on present-day Earth (Table 2) and 3.8 Ga seawater (Pope et al., 2012).

$F_{se} \gg F_{ch}$, and $F_{ch} \sim F_{we}$. Here we further assume $F_{de} = F_{re}$. Equations (3) and (4) are approximated as $f_{re} \sim f_{dehy}$ and $f_{ar} \sim 1$. Substituting these relations for Equations (A.1)–(A.3) gave,

$$\frac{I_o}{I_m} \sim \frac{f_{de}}{f_{se} f_{dehy}} \tag{A.4}$$

$$\frac{I_{cc}}{I_o} \sim \frac{f_{ch}}{f_{we}} \tag{A.5}$$

$$\frac{I_{oc}}{I_o} \sim f_{se}. \tag{A.6}$$

Therefore, we can derive,

$$\Delta D_{o-m} \sim 10^3 \ln f_{de} - 10^3 \ln f_{se} - 10^3 \ln f_{dehy} \tag{A.7}$$

$$\Delta D_{cc-o} \sim 10^3 \ln f_{ch} - 10^3 \ln f_{we} \tag{A.8}$$

$$\Delta D_{oc-o} \sim 10^3 \ln f_{se} \tag{A.9}$$

Substituting the fractionation factors (Table 1) gave $\Delta D_{o'-m} \sim 70‰$, $\Delta D_{cc-o'} \sim -80‰$, and $\Delta D_{oc-o'} \sim -30‰$, which is consistent with the δD values obtained from field samples (Table 2). Here an apostrophe denotes the fractionation from seawater before the correction by adding small reservoirs.

On the other hand, considering a water cycle without slab dehydration ($F_{re} \gg F_{ar}$) leads to a different steady state. In this case Equation (A.1) gave,

$$\frac{I_o}{I_m} \sim \frac{f_{de}}{f_{se}} \tag{A.10}$$

$$\Delta D_{o-m} \sim 10^3 \ln f_{de} - 10^3 \ln f_{se}. \tag{A.11}$$

Equation (A.11) led to $\Delta D_{o'-m} \sim 30‰$, which is smaller than the measurements (Table 2). These estimates showed that the isotopic fractionation due to slab dehydration is one of the important processes to explain the present-day D/H ratios in the mantle.

Appendix B. The constant-flux model

We demonstrated how the δD evolved toward a steady state (Appendix A) in Fig. 8. Here we assumed that all fluxes are balanced and two types of water cycle were investigated: $F_{de} = F_{ch} = F_{we} = 1/10$ $F_{se} = 1/10$ F_{ar} (the dehydration model) and $F_{de} = F_{se} = F_{re}$, $F_{ar} = F_{ch} = F_{we} = 0$ (the non-dehydration model). The dehydration model (Figs. 8a–c) evolved toward a steady state given by Equation (A.7), where $\Delta D_{o'-m} \sim 70‰$. On the other hand, the non-dehydration model (Fig. 8d) evolved toward a steady state given by Equation (A.11), where $\Delta D_{o'-m} \sim 30‰$.

The timescale to reach the steady state is determined by the residence time of water in the ocean and mantle, which is $\sim$10 Gyr in Fig. 8a, $\sim$2 Gyr in Figs. 8b and 8d, and $\sim$1 Gyr in Fig. 8c.

Appendix C. Supplementary material

Supplementary material related to this article can be found online at https://doi.org/10.1016/j.epsl.2018.06.016.

References

Armstrong, R., 1981. Radiogenic isotopes: the case for crustal recycling on a near-steady-state no-continental-growth Earth. Philos. Trans. R. Soc. Lond. A, Math. Phys. Eng. Sci. 301 (1461), 443–472.

H. Kurokawa et al. / Earth and Planetary Science Letters 497 (2018) 149–160

Bodnar, R.J., Azbej, T., Becker, S.P., Cannatelli, C., Fall, A., Severs, M.J., 2013. Whole Earth geohydrologic cycle, from the clouds to the core: the distribution of water in the dynamic Earth system. Spec. Pap., Geol. Soc. Am. 500, 431–461.

Catling, D.C., Zahnle, K.J., McKay, C.P., 2001. Biogenic methane, hydrogen escape, and the irreversible oxidation of early Earth. Science 293 (5531), 839–843.

Chacko, T., Riciputi, R., Cole, R., Horita, J., 1999. A new technique for determining equilibrium hydrogen isotope fractionation factors using the ion microprobe: application to the epidote–water system. Geochim. Cosmochim. Acta 63 (1), 1–10.

Clog, M., Aubaud, C., Cartigny, P., Dosso, L., 2013. The hydrogen isotopic composition and water content of southern pacific MORB: a reassessment of the D/H ratio of the depleted mantle reservoir. Earth Planet. Sci. Lett. 381, 156–165.

Dohm, J.M., Maruyama, S., 2015. Habitable trinity. Geosci. Front. 6 (1), 95–101.

Gaillard, F., Scaillet, B., Arndt, N.T., 2011. Atmospheric oxygenation caused by a change in volcanic degassing pressure. Nature 478 (7368), 229–232.

Graham, C.M., Harmon, R.S., Sheppard, S.M.F., 1984. Experimental hydrogen isotope studies: hydrogen isotope exchange between amphibole and water. Am. Mineral. 69, 128–138.

Hamano, K., Abe, Y., Genda, H., 2013. Emergence of two types of terrestrial planet on solidification of magma ocean. Nature 497 (7451), 607–610.

Harrison, T.M., 2009. The Hadean crust: evidence from >4 Ga zircons. Annu. Rev. Earth Planet. Sci. 37, 479–505.

Herzberg, C., Condie, K., Korenaga, J., 2010. Thermal history of the Earth and its petrological expression. Earth Planet. Sci. Lett. 292 (1), 79–88.

Hirschmann, M.M., 2006. Water, melting, and the deep Earth H_2O cycle. Annu. Rev. Earth Planet. Sci. 34, 629–653.

Höning, D., Hansen-Goos, H., Airo, A., Spohn, T., 2014. Biotic vs. abiotic Earth: a model for mantle hydration and continental coverage. Planet. Space Sci. 98, 5–13.

Höning, D., Spohn, T., 2016. Continental growth and mantle hydration as intertwined feedback cycles in the thermal evolution of Earth. Phys. Earth Planet. Inter. 255, 27–49.

Hren, M., Tice, M., Chamberlain, C., 2009. Oxygen and hydrogen isotope evidence for a temperate climate 3.42 billion years ago. Nature 462 (7270), 205.

Ito, E., Harris, D.M., Anderson, A.T., 1983. Alteration of oceanic crust and geologic cycling of chlorine and water. Geochim. Cosmochim. Acta 47 (9), 1613–1624.

Jarrard, R.D., 2003. Subduction fluxes of water, carbon dioxide, chlorine, and potassium. Geochem. Geophys. Geosyst. 4 (5).

Javoy, M., 2005. Where do the oceans come from? C. R. Géosci. 337 (1), 139–158.

Karato, S.-I., Jung, H., 2003. Effects of pressure on high-temperature dislocation creep in olivine. Philos. Mag. 83 (3), 401–414.

Kasting, J.F., Howard, M.T., Wallmann, K., Veizer, J., Shields, G., Jaffrés, J., 2006. Paleoclimates, ocean depth, and the oxygen isotopic composition of seawater. Earth Planet. Sci. Lett. 252 (1–2), 82–93.

Kharecha, P., Kasting, J., Siefert, J., 2005. A coupled atmosphere–ecosystem model of the early Archean Earth. Geobiology 3 (2), 53–76.

Kincaid, C., Sacks, I.S., 1997. Thermal and dynamical evolution of the upper mantle in subduction zones. J. Geophys. Res., Solid Earth 102 (B6), 12295–12315.

Korenaga, J., 2003. Energetics of mantle convection and the fate of fossil heat. Geophys. Res. Lett. 30 (8).

Korenaga, J., 2013. Initiation and evolution of plate tectonics on Earth: theories and observations. Annu. Rev. Earth Planet. Sci. 41, 117–151.

Korenaga, J., Planavsky, N.J., Evans, D.A., 2017. Global water cycle and the coevolution of the Earth's interior and surface environment. Philos. Trans. R. Soc. A 375 (2094), 20150393.

Kyser, T.K., O'Hanley, D.S., Wicks, F.J., 1999. The origin of fluids associated with serpentinization: evidence from stable-isotope compositions. Can. Mineral. 37 (1), 223–237.

Kyser, T.K., O'Neil, J.R., 1984. Hydrogen isotope systematics of submarine basalts. Geochim. Cosmochim. Acta 48 (10), 2123–2133.

Lécuyer, C., Gillet, P., Robert, F., 1998. The hydrogen isotope composition of seawater and the global water cycle. Chem. Geol. 145 (3), 249–261.

Lécuyer, C., Gruau, G., Früh-Green, G.L., Picard, C., 1996. Hydrogen isotope composition of early Proterozoic seawater. Geology 24 (4), 291–294.

Maruyama, S., Okamoto, K., 2007. Water transportation from the subducting slab into the mantle transition zone. Gondwana Res. 11 (1), 148–165.

McLennan, S.M., Taylor, S., 1982. Geochemical constraints on the growth of the continental crust. J. Geol. 90 (4), 347–361.

Mei, S., Kohlstedt, D., 2000. Influence of water on plastic deformation of olivine aggregates: 1. Diffusion creep regime. J. Geophys. Res., Solid Earth 105 (B9), 21457–21469.

Parai, R., Mukhopadhyay, S., 2012. How large is the subducted water flux? New constraints on mantle regassing rates. Earth Planet. Sci. Lett. 317, 396–406.

Peacock, S.M., 1993. Large-scale hydration of the lithosphere above subducting slabs. Chem. Geol. 108 (1), 49–59.

Pope, E.C., Bird, D.K., Rosing, M.T., 2012. Isotope composition and volume of Earth's early oceans. Proc. Natl. Acad. Sci. 109 (12), 4371–4376.

Schmidt, M.W., Poli, S., 1998. Experimentally based water budgets for dehydrating slabs and consequences for arc magma generation. Earth Planet. Sci. Lett. 163 (1), 361–379.

Schubert, G., Reymer, A., 1985. Continental volume and freeboard through geological time. Nature 316 (6026), 336–339.

Shaw, A., Hauri, E., Behn, M., Hilton, D., Macpherson, C., Sinton, J., 2012. Long-term preservation of slab signatures in the mantle inferred from hydrogen isotopes. Nat. Geosci. 5 (3), 224–228.

Shaw, A., Hauri, E., Fischer, T., Hilton, D., Kelley, K., 2008. Hydrogen isotopes in Mariana arc melt inclusions: implications for subduction dehydration and the deep-earth water cycle. Earth Planet. Sci. Lett. 275 (1), 138–145.

Sheppard, S.M., 1986. Characterization and isotopic variations in natural waters. Rev. Mineral. Geochem. 16 (1), 165–183.

Stevenson, D.J., Spohn, T., Schubert, G., 1983. Magnetism and thermal evolution of the terrestrial planets. Icarus 54 (3), 466–489.

Suzuoki, T., Epstein, S., 1976. Hydrogen isotope fractionation between OH-bearing minerals and water. Geochim. Cosmochim. Acta 40 (10), 1229–1240.

Taylor, H., 1974. The application of oxygen and hydrogen isotope studies to problems of hydrothermal alteration and ore deposition. Econ. Geol. 69 (6), 843–883.

Walker, J.C., 1977. Evolution of the Atmosphere. Macmillan/Collier Macmillan, New York/London.

Wenner, D.B., Taylor Jr, H.P., 1974. D/H and $^{18}O/^{16}O$ studies of serpentinization of ultramafic rocks. Geochim. Cosmochim. Acta 38 (8), 1255–1286.

Young, G.M., Brunn, V.V., Gold, D.J., Minter, W., 1998. Earth's oldest reported glaciation: physical and chemical evidence from the Archean Mozaan Group (∼2.9 Ga) of South Africa. J. Geol. 106 (5), 523–538.